FREQUENCY = 2.05 GHz
PEAK GAIN = 12.0 dBic
A.R. = 0.8 dB
B.W. = 46°

Figure 8

is 8.5 by 8.5 in., including the printed microstrip transmission lines. Figure 8 illustrates a representative measured radiation pattern from this array. The measured array performances are summarized in Table 2. Clearly, the sequentially fed array gives better VSWR bandwidth, axial ratio, and side-lobe level (−24 dB SLL) performance than the conventional feed array. Due to the smaller element spacing for the sequential feed array, the peak gain is slightly lower than the conventional feed array. Note that the antenna size may be further reduced to approximately 6 by 6 in. in size by replacing the feed lines with a PCB feed circuit board behind the radiating patch elements.

CONCLUSION

Two different low-gain omni antennas (the drooping dipole and the TM_{21}-mode circular patch antennas), and two medium gain patch antennas were developed for the successful DBSR demonstrations in Pasadena, California and Buenos Aires, Argentina. These low-cost antennas can be used either indoors or outdoors to receive digital audio signals from the TDRSS satellite. The patch antennas are more conformal than the drooping dipole antennas. For the medium gain antenna, the sequentially arranged CP fed array has a better CP performance over a broader bandwidth than the conventionally fed array. Finally, these antennas have myriad applications in modern satellite or wireless communication systems, such as MSAT, INMARSAT, IRIDIUM, Globalstar, Odyssey, Geostar, etc.

TABLE 2 Summary of Medium Gain Antenna Performance at 2.05 GHz

Array Type	Conventional Feed	Sequential Feed
Peak gain (dBic)	13.7	12.0
VSWR	1.13	1.48
Bandwidth (MHz)	82	132
Beamwidth (Deg.)	38	46
Side-lobe level (dB)	−13	−24
Axial ratio (dB)	1.4	0.8

REFERENCES

1. K. Woo et al., "Performance of a Family of Omni and Steered Antennas for Mobile Satellite Applications," *Proc. IMSC*, Ottawa, Canada, 1990, pp. 540–546.
2. J. Huang, "Circularly Polarized Conical Patterns from Circular Microstrip Antennas," *IEEE Trans. Antennas Propagat.*, Vol. AP-32, No. 9, Sept. 1984, pp. 991–994.
3. M. Haneishi and Y. Suzuki, "Circular Polarization and Bandwidth," in J. R. James and P. S. Hall, *Handbook of Microstrip Antennas*, Peter Peregrinus Ltd., London, Chap. 4, p. 220.
4. R. E. Munson, "Microstrip Antennas," in R. C. Johnson (Ed.), *Antenna Engineering Handbook* (3rd ed.), McGraw-Hill, New York, 1993, pp. 7–16.
5. J. Huang, "A Technique for an Array to Generate Circular Polarization with Linearly Polarized Elements," *IEEE Trans. Antennas Propagat.*, Vol. AP-34, pp. 1113–1124, Sept. 1986.
6. T. Teshirogi et al., "Wideband Circularly Polarized Array Antenna with Sequential Rotations and Phase Shifts of Elements," *Proc. Int. Symp. on Ant. and Propag.*, Japan, 1985, pp. 117–120.

A FINITE-ELEMENT ANALYSIS OF BENDING DIELECTRIC WAVEGUIDES WITH REFLECTION WALLS

Shyh-Jong Chung
Department of Communication Engineering
National Chiao Tung University
Hsinchu, Taiwan, Republic of China

KEY TERMS

Bending dielectric waveguide, reflection wall, finite-element method, Green's function

ABSTRACT

The finite-element method together with the Green's-function technique is employed to tackle the scattering problems of bending dielectric waveguides with reflection walls. The influences of the frequency, the ratio of waveguide widths, and the length of the reflection wall on the scattering characteristics of 90° and 120° bends are presented. © 1994 John Wiley & Sons, Inc.

I. INTRODUCTION

Bending dielectric waveguides are basic elements to integrated circuits operating in the range from millimeter wave to optical frequencies. They are necessary in order to reduce the large length–width ratio of waveguide chips consisting of several coupled devices. Two types of bending waveguides have been proposed: curved bending waveguides and sharp bending waveguides (corner bends). The latter have the ad-

vantage of small bending radius and thus are used for compact guided-wave circuits.

A sharp bending waveguide structure consists of two differently directed semi-infinite waveguides with the ends joined together (which make a corner). When a guided mode of one of the waveguides is incident toward the corner, some of the power is reflected back to the same waveguide, and some is transmitted to the other waveguide, both carried by the guided modes of the waveguides. In addition to these two mechanisms, the rest power is radiated to the surroundings, which may interfere with the nearby components. In order to reduce the radiated power and increase the transmitted power, a number of alternative structures including reflection walls are proposed. The reflection wall is made by reactive-ion etching [1] or wet-chemical etching [2] at the corner so that a mirrorlike facet is formed. When the power is incident upon the reflection wall, either total internal reflection or large partial reflection occurs at the facet, which greatly increases the transmission power.

For the analysis of bending waveguides, the effective dielectric constant (EDC) method has been adopted to reduce the original three-dimensional structure into a two-dimensional one for the purpose of simplicity. Marcatili [3] derived a transcendental relation for the attenuation per radian in a curved waveguide. Numerical results based on the EDC analysis of Furuta, Noda, and Ihaya [4] and curves presented by Marcatili show that the difference Δn in the effective refractive index between the waveguide core and its surroundings has to be at least 0.01 for acceptable radiation losses of 1 dB/rad and that a radius of curvature of a few millimeters is required. Himeno, Terui, and Kobayaahi [5] used the plane-wave-spectrum method and considered the Goos-Hanchen effect to handle the wave reflection at the bend (with reflection wall). Morita [6] matched the tangential field at a boundary passing through the corner of the bend, and iteratively solved the scattering problem. Although Morita's method is more rigorous than Himeno's, it looks that the results are difficult to converge as the difference of the refractive indices becomes large. Furthermore, Morita's method fails to tackle the problems of bends with reflection walls. Tanaka and Kojima [7] developed a form of volume integral equation for the treatment of wave propagation in two-dimensional dielectric branching waveguides, and then solved it by the method of moments. Although this method can be used to handle the scattering problem of bending waveguides, it will be CPU time consuming because of the calculations of the Green's function for all the nodes in the entire waveguide region.

In this study a variational equation solved by the finite-element method is derived for rigorously analyzing the characteristics of bending waveguides with reflection walls. The variations of the reflection and transmission coefficients as well as the radiation power are investigated by changing the frequency, the ratio of the waveguide widths, and the length of the reflection wall.

II. ANALYSIS

Figure 1 shows a waveguide bend formed by two dielectric waveguides with widths of $2d_1$ and $2d_2$. The bend angle is 2θ and the effective refractive indices are n_c in the core region and n_d in the surrounding (cladding) region. The two waveguides are both assumed to be single moded. Let the TE propagation mode of the left-hand side (LHS) waveguide be incident upon the bend. Due to the uniformity of the structure
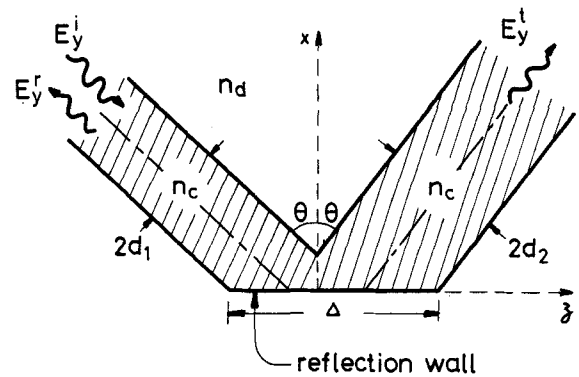

Figure 1 A bending dielectric waveguide with a reflection wall

in the y direction, the total electric field is only of y component.

To tackle the problem by the finite-element method, one encloses a finite region Ω by the boundaries B_i's, $i = 1, 2, 3, 4$, as shown in Figure 2. The boundaries B_1 and B_3 are chosen far away from the corner so that only propagation modes can exit at these boundaries. By the partial variation principle [8], a variational equation can be derived as follows:

$$\delta^a(\omega\mu_0 I^a) = 0,$$

$$\begin{aligned}
\omega\mu_0 I^a = -j \int_\Omega dv \left(k_o^2 n^2(x, z)E_y^a E_y \right. \\
\left. - \frac{\partial E_y^a}{\partial x}\frac{\partial E_y}{\partial x} - \frac{\partial E_\omega^a}{\partial z}\frac{\partial E_y}{\partial z} \right) \\
+ \oint_{\Sigma B_i} ds\ E_y^a(B_i^-) \cdot (\hat{y} \times \hat{n}) \cdot w\mu_0\overline{H}(B_i^+) \\
+ \oint_{\Sigma B_i} ds(\hat{y} \times \hat{n}) \cdot w\mu_0\overline{H}^a(B_i^+) \\
\times [E_y(B_i^-) - E_y(B_i^+)],
\end{aligned} \tag{1}$$

where the variational operator δ^a operates only on the terms with superscript a and $n(x, z)$ is the distribution of the refractive index in Ω, which equals n_c in the core region and n_d in the cladding region. $\hat{n}$ denotes the outward normal of the boundaries B_i's. B_i^+ and B_i^- represent the surfaces just exterior and interior to the boundary B_i, respectively.

To solve (1) the region Ω is divided into various triangular elements as shown in Figure 2. It is noticed that the boundaries
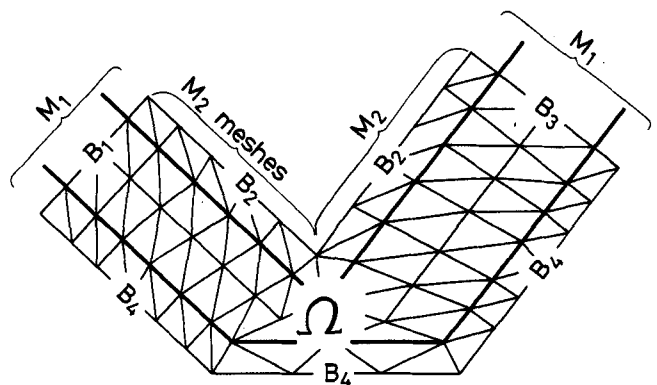

Figure 2 An enclosed finite-element regain Ω and the mesh division with triangular elements

B_2 and B_4 are set one mesh apart from the waveguide boundaries to avoid handling the singularity of the Green's function in the later formulation. Two groups of fields are involved in (1), that is, those interior and exterior to the closed boundary ΣB_i. The former includes the fields in the volume integral and the fields at B_i^- in the surface integral; the latter consists of those at B_i^+ in the surface integral.

The interior field E_y^e at the eth triangular element is expanded by the nodal field values ϕ_i^e's and the corresponding second-order shape functions N_i's [9]:

$$E_y^e(x, z) = \sum_{i=1}^{6} \phi_i^e N_i, \qquad (2)$$

where six nodes are specified for each triangular element.

The exterior fields are obtained through the use of the equivalent current J_y at the core region:

$$E_y(x, y) = -j\omega\mu_0 \int_{\text{core}} J_y(x', z')G(x, z; x', z') \, dv'$$

$$= k_0^2(n_c^2 - n_d^2) \int_{\text{core}} E_y(x', z')G(x, z; x', z') \, dv', \qquad (3)$$

where the equality $J_y = j\omega\epsilon_0(n_c^2 - n_d^2)$ has been used. $G(x, z; x', z') = 1/4j \, H_0^{(2)}$ is the 2D Green's function for the homogeneous medium n_d, with $k_d = k_0 n_d$ and

$$\rho = \sqrt{(x - x')^2 + (z - z')^2}.$$

The integration range in (3), that is, the core region, can be divided into three parts: the first part is the core region inside Ω; the second and the third parts are the core regions of LHS and right-hand-side (RHS) waveguides, respectively, outside Ω. The field $E_y(x', z')$ of the first part is represented as the form of (2). The field of the second part consists of the incident and the reflected modal fields of the LHS waveguide:

$$E_y(x_1, z_1) = (e^{-j\beta_1 z_1} + Re^{j\beta_1 z_1})u_1(x_1). \qquad (4)$$

Finally, the field of the last part is the transmitted modal field of the RHS waveguide:

$$E_y(x_2, z_2) = Te^{-j\beta_2 z_2}u_2(x_2). \qquad (5)$$

Here (x_i, z_i) is the local coordinate for the LHS waveguide $(i = 1)$ or the RHS waveguide $(i = 2)$ (with z_i being the longitudinal direction of the waveguide). β_i and u_i are the propagation constant and the modal function. R and T are the reflection coefficient and transmission coefficient, respectively, which are unknowns. It is noticed that by using the asymptotic form of the Green's function, the integrations for the second and third parts can be analytically carried out.

By casting the field representations of (2) and (3) into (1) and using the Galerkin-Ritz procedure, one gets a matrix equation of the form

$$\overline{\overline{A}} \, \overline{x} = \overline{b}. \qquad (6)$$

The unknown vector $\overline{x} = [\phi_i^e\text{'s}, R, T]^T$ is obtained after inverting (6), and the radiation field is then calculated from (3).

TABLE 1 Convergence Test of Reflection (R) and Transmission (T) Coefficients of a Bending Waveguide.
$2\theta = 120°$, $k_0 d_1 = k_0 d_2 = 0.2$, $\Delta = 4d_1$, $k_0 L_1 = k_0 L_2 = 10$

| M_1	M_2	R	T
3	10	$0.059 \angle -161.3°$	$0.646 \angle 6.0°$
3	15	$0.059 \angle -160.6°$	$0.645 \angle 5.9°$
3	20	$0.059 \angle -160.3°$	$0.645 \angle 5.8°$
4	20	$0.058 \angle -160.1°$	$0.646 \angle 5.4°$

III. NUMERICAL RESULTS

In this section some numerical results are presented under the specification of $n_c = 2.2$ and $n_d = 1$. As a convergence test of the present approach, Table 1 shows the scattering coefficients R and T for several mesh divisions. M_1 and M_2 are the meshes along the transverse and longitudinal directions of the waveguides (Figure 2). L_1 and L_2 are the distances from the boundaries B_1 and B_3, respectively, to the origin of the global coordinate. The convergence of the magnitudes and phases of the coefficients verifies the validity of the present work.

As a further check of the analysis, Figure 3 illustrates the magnitudes of the electric fields exterior (solid line) and interior (dash lines) to the boundaries B_i's. The interior field is obtained from the finite-element nodal values along the boundaries, and the exterior one is calculated based on the equivalent source in the core region and the Green's function (3). It is seen that the field magnitudes match very well along the whole boundaries. Although not shown, the phases of the fields also match well with the difference below 1 degree.

Figure 4 shows the scattering coefficients (R, T) and the total radiation powers P_{rad} for 90°- and 120°-bend structures, as a function of the normalized frequency $k_0 d_1$. Power-conservation law $(|R|^2 + |T|^2 + P_{\text{rad}} = 1)$ is satisfied to within 0.1% error for each point calculated. Note that the transmission coefficient T increases with the width of the waveguide. This is because as $k_0 d_1$ increases, the guided mode has more field concentrated in the core region, so that more power meets the reflection wall and is transmitted to the other wave-
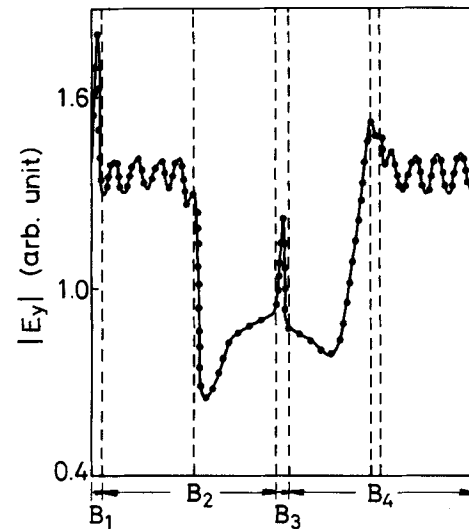
Figure 3 Magnitude of the electric field along the boundaries B_i's. Dotted line, interior field; solid line, exterior field. $2\theta = 120°$. $k_0 d_1 = k_0 d_2 = 0.2$, $\Delta = 4d_1$, $k_0 L_1 = k_0 L_2 = 10$. $M_1 = 3$, $M_2 = 20$
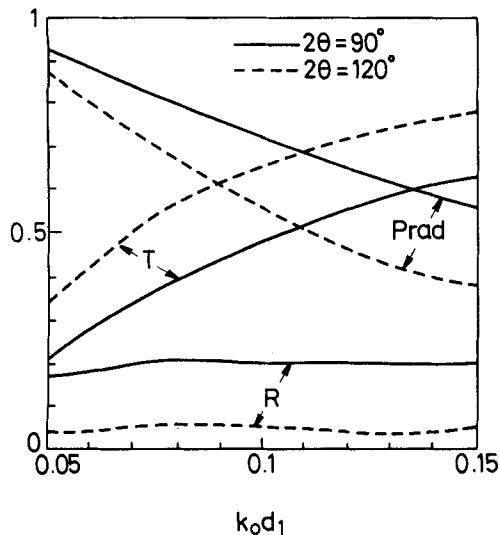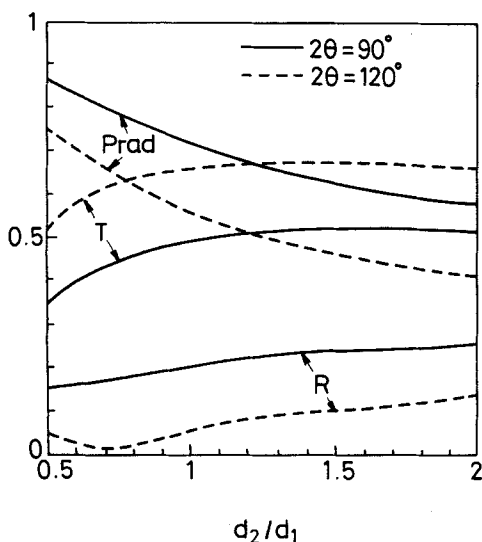
Figure 4 Scattering coefficients and radiation powers as a function of k_0d_1. $d_2 = d_1$, $\Delta = 2d_1/\cos\theta$, $k_0L_1 = k_0L_2 = 20$. $M_1 = 3$, $M_2 = 20$
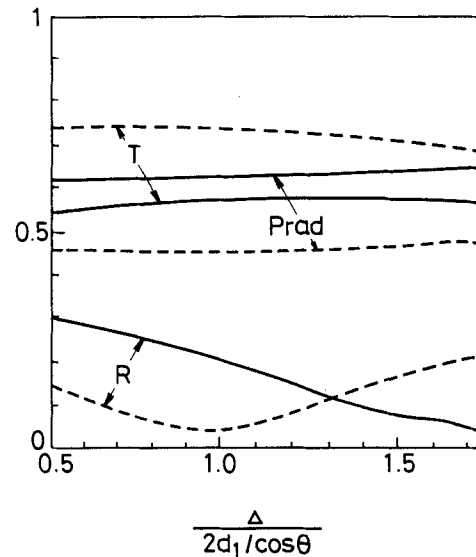

Figure 6 Scattering coefficients and radiation powers as a function of $\Delta/(2d_1/\cos\theta)$. $k_0d_1 = k_0d_2 = 0.125$, $k_0L_1 = k_0L_2 = 20$. $M_1 = 3$, $M_2 = 20$

guide. It is also noticed that increasing k_0d_1 seems to have little influence on the reflection coefficient for both 90° and 120° bends.

Figure 5 depicts the scattering coefficients and radiation powers as a function of d_2/d_1 for 90° and 120° bends. d_1 is kept constant, and d_2 is varied. Because the width of the reflection wall changes proportional to d_2, the increase of d_2 enhances the transmission coefficients. But as d_2 becomes larger than $1.25d_1$, the transmission coefficients reach saturation values because further increase of d_2 (or the width of the reflection wall) has little influence on the reflection of the incident field, which has a constant field width.

Figure 6 presents the dependences of the scattering coefficients and radiation powers on the width Δ of the reflection wall. $\Delta/(2d_1/\cos\theta)$ equals zero when the reflection wall vanishes, and equals two when the wall touches the connecting point of the upper boundaries of the waveguides. For the parameters chosen, the variation of Δ does not change the transmission coefficients and radiation powers much, but has

large influence on the reflection coefficients. It is seen from the figure that the reflection coefficient of the 90° bend decreases monotonically with the increase of Δ and that of the 120° bend has a minimum value around the point $\Delta/(2d_1/\cos\theta) = 1$.

IV. CONCLUSIONS

A method combining the finite-element approach and the Green's-function technique has been presented to solve the scattering problems of bending dielectric waveguides with reflection walls. The validity of this method has been checked by convergence test and by field matching at the finite-element boundary. Several numerical results for 90° and 120° bends have been analyzed and discussed. With a little modification, this method can be applied to tackle the scatterings of branching waveguides or intersecting waveguides.

REFERENCES

1. P. Buchmann and H. Kaufmann, "GaAs Single-Mode Rib Waveguides with Reactive Ion-Etched Totally Reflecting Corner Mirrors," *J. Lightwave Technol.*, Vol. LT-3, Aug. 1985, pp. 785–788.
2. T. M. Benson, "Etched-Wall Bent-Guide Structure for Integrated Optics in the III-V Semiconductors," *J. Lightwave Technol.*, Vol. LT-2, Feb. 1984, pp. 31–34.
3. E. A. J. Marcatili, "Bends in Optical Dielectric Guides," *Bell Syst. Tech. J.*, Sept. 1969, pp. 2103–2132.
4. H. Furuta, H. Noda, and A. Ihaya, "Novel Optical Waveguide for Integrated Optics," *Appl. Opt.*, Vol. 13, 1974, p. 322.
5. A. Himeno, H. Terui, and M. Kobayashi, "Loss Measurement and Analysis of High-Silica Reflection Bending Optical Waveguides," *J. Lightwave Technol.*, Vol. 6, Jan. 1988, pp. 41–46.
6. N. Morita, "A Rigorous Analytical Solution to Abrupt Dielectric Waveguide Discontinuities," *IEEE Trans. Microwave Theory Tech.*, Vol. MTT-39, Aug. 1991, pp. 1272–1278.

Figure 5 Scattering coefficients and radiation powers as a function of d_2/d_1. $k_0d_1 = 0.1$, $\Delta = 2d_1/\cos\theta$, $k_0L_1 = k_0L_2 = 20$. $M_1 = 3$, $M_2 = 20$

7. K. Tanaka and M. Kojima, "Volume Integral Equations for Analysis of Dielectric Branching Waveguide," *IEEE Trans. Microwave Theory Tech.*, Vol. MTT-36, Aug. 1988, pp. 1239–1245.

8. S.-J. Chung and C. H. Chen, "Partial Variational Principle for Electromagnetic Field Problems: Theory and Application," *IEEE Trans. Microwave Theory Tech.*, Vol. MTT-36, March 1988, pp. 473–479.

9. O. C. Zienkiewicz, *The Finite Element Method*, McGraw-Hill, New York, 1977.

SPECTRAL ELECTRIC GREEN'S DYAD FOR A GROUNDED BIANISOTROPIC SLAB FED BY A THREE-DIMENSIONAL POINT SOURCE

Alessandro Toscano and Lucio Vegni
Department of Electronic Engineering
Third University of Rome
Via Eudossiana 18
00184 Rome, Italy

KEY TERMS
Pseudochiral material, point-source antenna, Green's dyad

ABSTRACT

The subject of this article is the analysis of planar stratified structures with a general bianisotropic grounded slab fed by a three-dimensional electric point source. The electromagnetic problem is solved in terms of the spectral electric Green's dyad. The elements of the first and third column of the spectral Green's dyad are directly derived from the transmission line equations satisfied by the electromagnetic field in the two-dimensional Fourier domain. The reaction theorem and the Parseval theorem are then applied to the spectral electromagnetic field, and the elements of the second column of the spectral Green's dyad are provided. Finally, as an application of the theory, we present the expression of the $\bar{G}_{yy}$ term when the bianisotropic grounded slab is a pseudochiral one. © 1994 John Wiley & Sons, Inc.

1. INTRODUCTION AND FORMULATION OF THE PROBLEM

Let us consider a planar integrated structure (Figure 1) formed by a grounded, linear bianisotropic slab, in the presence of
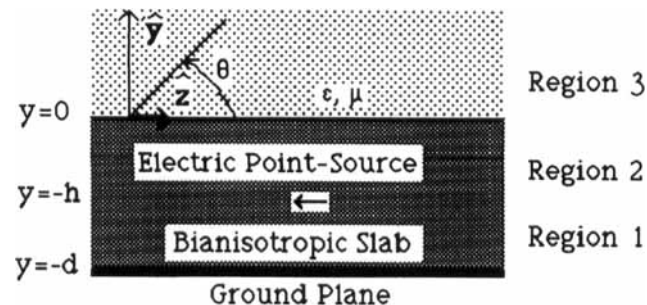

Figure 1 Planar grounded slab fed by an electric point source

an isotropic half space, fed by an electric point source located inside the slab:

$$\mathbf{J} = \delta_0(x)\,\delta_0(y + h)\,\delta_0(z)(J_x\hat{x} + J_y\hat{y} + J_z\hat{z}), \qquad (1)$$

where $\delta_0(x)$ is the Dirac delta function.

The distribution of the electromagnetic field in the structure under examination can be obtained in a complete and exact way through the determination of the spectral electric Green's dyad [1, 2]. The elements of the first and third column of the dyad may be derived in a straightforward manner by making use of the equivalent transmission lines. To this end, in the two-dimensional Fourier domain defined as

$$\tilde{\Psi}(\alpha, y, \beta) = \int_{-\infty}^{+\infty}\int_{-\infty}^{+\infty} \Psi(x, y, z)e^{j(\alpha x + \beta z)}\, dx\, dz,$$

$$\Psi(x, y, z) = \frac{1}{4\pi^2}\int_{-\infty}^{+\infty}\int_{-\infty}^{+\infty} \tilde{\Psi}(\alpha, y, \beta)e^{-j(\alpha x + \beta z)}\, d\alpha\, d\beta \qquad (2)$$

the electromagnetic field has been decomposed as a superposition of $\mathbf{TE}(\hat{y})$ and $\mathbf{TM}(\hat{y})$ waves whose transverse components satisfy the transmission-line equations. We found that such a decomposition is always possible when the constitutive tensors of the medium satisfy the following symmetry conditions:

$$\boldsymbol{\varepsilon} = \begin{bmatrix} \varepsilon_{xx} & 0 & \varepsilon_{xz} \\ 0 & \varepsilon_{yy} & 0 \\ \varepsilon_{zx} & 0 & \varepsilon_{zz} \end{bmatrix}, \qquad \boldsymbol{\sigma}_{em} = \begin{bmatrix} 0 & \sigma_{xy} & 0 \\ \sigma_{yx} & 0 & \sigma_{yz} \\ 0 & \sigma_{zy} & 0 \end{bmatrix},$$

$$\boldsymbol{\tau}_{me} = \begin{bmatrix} 0 & \tau_{xy} & 0 \\ \tau_{yx} & 0 & \tau_{yz} \\ 0 & \tau_{zy} & 0 \end{bmatrix}, \qquad \boldsymbol{\mu} = \begin{bmatrix} \mu_{xx} & 0 & \mu_{xz} \\ 0 & \mu_{yy} & 0 \\ \mu_{zx} & 0 & \mu_{zz} \end{bmatrix}, \qquad (3a)$$

being

$$\mathbf{D} = \boldsymbol{\varepsilon} \cdot \mathbf{E} + \boldsymbol{\sigma} \cdot \mathbf{H},$$

$$\mathbf{B} = \boldsymbol{\tau} \cdot \mathbf{E} + \boldsymbol{\mu} \cdot \mathbf{H}. \qquad (3b)$$

Once the transmission-line problems for the $\mathbf{TE}(\hat{y})$ and $\mathbf{TM}(\hat{y})$ spectral waves have been solved, the elements of the first and third column of the spectral electric Green's dyad are given by

$$\begin{bmatrix} \tilde{G}_{xx,k} \\ \tilde{G}_{zz,k} \end{bmatrix} = G_k^{\text{TM}}\begin{bmatrix} \sin^2\delta \\ \cos^2\delta \end{bmatrix} + G_k^{\text{TE}}\begin{bmatrix} \cos^2\delta \\ \sin^2\delta \end{bmatrix},$$

$$\tilde{G}_{xz,k} = \tilde{G}_{xz,k} = (G_k^{\text{TM}} + G_k^{\text{TE}})\sin\delta\cos\delta$$

$$(k = 1, 2, 3),$$

$$\begin{bmatrix} \tilde{G}_{yx,k} \\ \tilde{G}_{yz,k} \end{bmatrix} = \frac{Z_{y,k}}{Z_k^{\text{TM}}} G_k^{\text{TM}}\begin{bmatrix} \sin\delta \\ \cos\delta \end{bmatrix}, \qquad (4a)$$

where

$$\sin\delta = \frac{\alpha}{\sqrt{\alpha^2 + \beta^2}}, \qquad \cos\delta = \frac{\beta}{\sqrt{\alpha^2 + \beta^2}},$$

$$\xi = \sqrt{\alpha^2 + \beta^2}, \qquad (4b)$$

$$\begin{bmatrix} G_1^{(\text{TE,TM})} \\ G_2^{(\text{TE,TM})} \\ G_3^{(\text{TE,TM})} \end{bmatrix} = \frac{Z_1^{(\text{TE,TM})}}{F_1^{(\text{TE,TM})}(d)}\begin{bmatrix} F_1^{(\text{TE,TM})}(h)\,\sinh[k_y(d + y)] \\ F_1^{(\text{TE,TM})}(y)\,\sinh[k_y(d - h)] \\ Z_2^{(\text{TE,TM})}e^{-k_2 y}\,\sinh[k_y(d - h)] \end{bmatrix},$$

$$(4c)$$